Controllability of Magnetic Force in Magnetic Wheels

Kyung-Hyun Yoon and Young-Woo Park

Department of Mechatronics Engineering, Chungnam National University, Yuseong-gu, Daejeon 305-764, Korea

Magnetic adhesion on mobile robots has advantages such as fast locomotion and no additional energy for adhesion process, and one definite disadvantage like difficulty to control magnetic force. This paper focuses on this issue, i.e., controllable magnetic force, and describes the design of a magnetic wheel using two permanent magnets (PMs) for controlling magnetic force between the wheel and interior surfaces of ferromagnetic pipes. It is composed of a central PM, one aluminum ring, two wheel rims, and one housing. The housing also has a rotatable PM which is connected to a servo motor via two pulleys and a timing belt. A commercial program, MAXWELL-3D, is used to model and analyze the magnetic wheel. Then, the wheel is made and is subjected to the experiments. From the simulation results, the flux lines are thicker as the PM2 rotates from free-state to adhered-state, which means that more magnetic flux flow through the steel pipe. A digital push-pull force gauge is used to measure the magnetic force by pulling the magnetic wheel vertically. It can be concluded that the proposed method is effective to control magnetic force between the wheel and interior surfaces of ferromagnetic pipes.

Index Terms—**Controllable magnetic forces, permanent magnets, magnetic wheel, MAXWELL-3D.**

I. Introduction

MOBILE robots can be categorized with respect to the locomotive mechanism or with respect to the adhesion mechanism because both are important issues in designing a mobile robot. They can be classified into five categories in terms of the adhesion aspects: suction type, magnetic type, gripping type, rail-guided type, and biomimetic type [1]. Among them, the magnetic adhesion on mobile robots has advantages such as fast locomotion and no additional energy for adhesion process, and one definite disadvantage is difficulty to control magnetic force at will.

The idea of using magnetic elements or wheels on mobile robots is not new. Tache *et al.* developed a mobile robot with adaptive magnetic wheels integrating a lifting and stabilizing mechanism, but used a mechanical lifter to control magnetic force [2]. This kind of the magnetic wheel may be beneficial for negotiating complex obstacles, but may be harmful for moving inside pipe. This disadvantage comes from the constant interaction between the magnetic wheel and interior surface of the ferromagnetic pipes. Fischer [3] and Kawaguchi [4] robots implemented a special mechanism to negotiate specific complex obstacles. The first is designed for vertical walls and the outer surfaces of pipes. They aim to pass difficult obstacles such as sharp ridges which do not provide magnetic attraction force, but these robots require a large gap and many degrees of freedom (DOF). In a newly suggested design, the magnetic flux enhances the adhesive force during the attachment while induction pins redirect magnetic flux in order to achieve an easier detachment, but it is hard to push and to pull the induction pin [5].

Reviewing previous work on magnetic wheels for mobile robots reveals that no magnetic wheels exist with continuously controllable magnetic forces. Thus, this paper focuses on this issue, i.e., continuously controllable magnetic force, and describes the design of a magnetic wheel using two permanent magnets (PMs) for controlling magnetic force between the wheel and interior surfaces of ferromagnetic pipes.

Manuscript received March 02, 2012; revised April 26, 2012, May 06, 2012; accepted May 06, 2012. Date of current version October 19, 2012. Corresponding author: Y. W. Park (e-mail: ywpark@cnu.ac.kr).

Color versions of one or more of the figures in this paper are available online at http://ieeexplore.ieee.org.

Digital Object Identifier 10.1109/TMAG.2012.2200240

II. Design and Fabrication

A. Concept

The basic idea of the magnetic wheels with controllable magnetic force is borrowed from a magnetic base, which is a magnetic fixture based on a magnet that can effectively be turned on and off at will. This magnetic base is made from two blocks of iron, which are combined with a non-ferrous material such as brass or aluminum. Then, a round cavity is bored through the enter. A round permanent magnet (PM) is inserted into the bored hole and a handle is attached to allow easy rotation of the magnet. The rotation of the PM changes the direction of the magnetic field so that it is either directed into the two halves, where the iron blocks act as keepers (free-state), or directed so that the field transverse the nonferrous material between the two halves, where the iron blocks act as an extension of the PM (adhered-state). In the case of the magnetic base, the PM can be rotated manually for the attachment or detachment to ferromagnetic surface.

B. Magnetic Wheel With Controllable Magnetic Force

Fig. 1 shows the concept of the magnetic wheel with controllable magnetic force, which is composed of a central PM (PM1), an aluminum ring, two wheel rims, and one housing with a rotatable PM (PM2). Fig. 1(a) and (b) show adhered and free states, respectively. Neglecting leakage, two sets of magnetic flux loops are formed: one consists of the PM2 and housing (Loop 1), and the other includes the PM1 and wheel rims (Loop 2).

In the free-state, the PMs in the wheel and in the housing are arranged with antiparallel poles, and designated as 0°. In this case, it indicates that the most magnetic flux is directed into PM2 instead of the steel pipe, as labeled Loop 2. This means that the iron wheel rims and PM2 act as the keeper and the extension, respectively.

In the adhered-state, the PMs in the wheel and in the housing are arranged with parallel poles, and designated as 180°. The

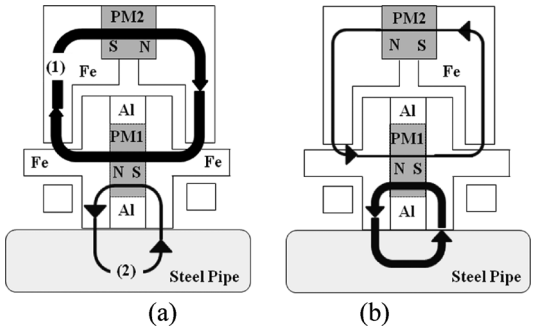

Fig. 1. Concept of the proposed magnetic wheel. (a) Free-state. (b) Adhered-state.

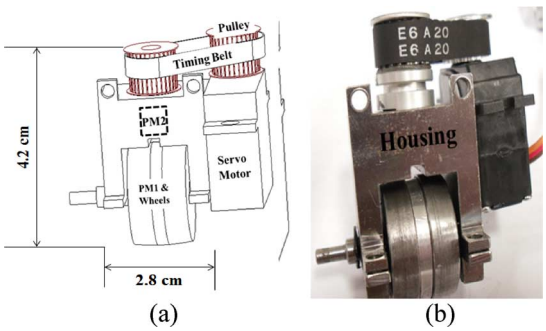

Fig. 2. Magnetic wheel. (a)3-D modeled. (b) Fabricated.

most magnetic flux from PM1 is directed into the surface of the steel pipe, as a labeled Loop 1. This means that the iron wheel rims and PM2 act as the extension and the keeper of the PM1, respectively. The magnetization of both PMs is axial so that the magnetic flux is closed through the wheel rims and the contact surface.

C. Fabrication

Fig. 2 shows the 3-D modeled and fabricated magnetic wheel. Both PMs are made of NdFeB with 35 MGOe. Both wheel rims and housing are made of a stainless steel, SUS430. An aluminum ring is used to block the interaction of the magnetic flux between PM1 and PM2. A servo motor coupled with two pulleys and one timing belt is used to rotate PM2 whenever a controllable magnetic force is needed. The selection criteria for the servo motor are based on the angle to be rotated and on the size compactness.

The wheel size is determined by considering the curvature of the pipe. The geometric constraint between the pipe curvature and the outer end of the wheel rim axis is the major factor to determine the size of a wheel. The wheel rim size is calculated as a diameter of 2.5 cm and the weight of the whole wheel is measured as 130 g.

III. Simulation and Experimental Procedure

A. MAXWELL-3D Simulation

A commercial program, MAXWELL-3D, is used to model and analyze the magnetic wheel. The material properties for the

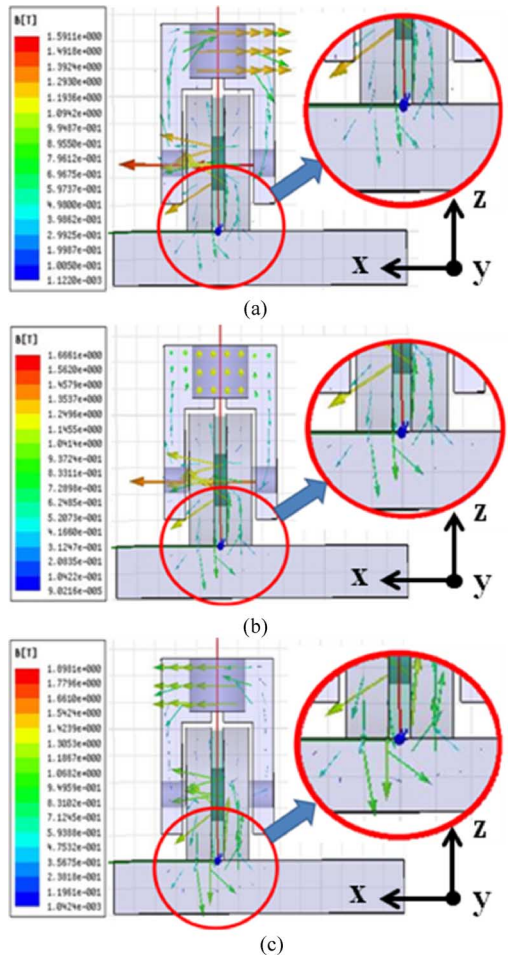

Fig. 3. MAXWELL-3D simulation. (a)Free-state. (b) Mid-state. (c) Adhered-state.

respective PMs and SUS430 are input as a form of B–H curves. Two sets of simulation are planned and performed: one with an interval of 15° from 0° to 180°, and the other with a gap interval of 0.1 mm from 0 to 0.5 mm. The former simulation is to see the effect of the rotation of the PMs, while the latter is to see the effect of the gap between the wheel rim and the interior surface of the steel pipe, and to use later for the compensation of the experimental data.

To show the magnetic flux line clearly, a magnetically analyzed wheel is aligned along the y-axis which is the direction protruding from the paper.

Fig. 3 shows some of the simulation results with the flux lines. In the figure, the interaction between the PM1 and steel pipe is enlarged and shown in the circle. From Fig. 3(a), it is clear that the stronger magnetic flux loop is formed around PM2 than the magnetic flux loop around PM1. Because PM1 and PM2 are positioned to have antiparallel poles, the most magnetic flux from PM1 can flow through PM2 instead of the steel pipe. The maximum flux density on the wheel is around 0.71 T. From Fig. 3(b), it is seen that the magnetic flux lines are twisted, and that the magnetic flux loops around PM1 and around PM2 look similar. Since the pole of the PM2 is positioned along the y-axis, the interaction of the magnetic flux lines between PM1 and PM2

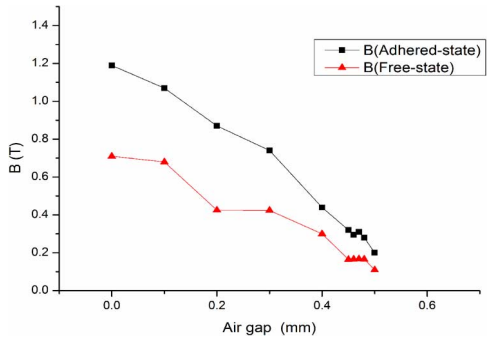

Fig. 4. Flux density variation to the change of gap.

causes the twisted magnetic flux lines. The maximum flux density on the wheel is around 0.83 T. From Fig. 3(c), it is seen that the magnetic flux loop is formed around PM1. Because PM1 and PM2 are positioned to have parallel poles, the most magnetic flux from PM1 flows through the steel pipe instead of PM2. The maximum flux density on the wheel is around 1.19 T. From the enlarged view in the right circle, the flux lines thicken as the PM2 rotates from the free-state to the adhered-state. This means that more magnetic flux flows through the steel pipe.

Fig. 4 shows the variation of flux density to the change of a gap in simulation. The flux density decreases as a gap increases. These data are used to derive the compensation equations for the adhered-state and free-state. The relation between the gap (X) and flux density (Y) at the adhered-state and at the free-state is represented as the (1) and (2), respectively

$$Y_{\text{free}} = -1.2X + 0.71 \quad (1)$$

$$Y_{\text{adhered}} = -1.96X + 1.19 \quad (2)$$

where Y_{free} and Y_{adhered} are flux density with free-state and adhered-state in simulation. X is gap.

Substituting 0.5 as a value of X and experimental flux density at $\mathrm{X} = 0.5$ into (1) and (2) yields

$$Y_{\text{free}} = -1.2X + 0.67 \quad (3)$$

$$Y_{\text{adhered}} = -1.96X + 1.15. \quad (4)$$

Using (3) and (4), the flux density at a gap of 0 mm can be estimated and regarded as experimental data.

B. Experimental Procedure

Two sets of experiments are planned to characterize the developed magnetic wheel: one for the magnetic flux density measurements, and the other for magnetic force. Figs. 5 and 6 show the respective experimental setup. For the former experiments, a gauss meter is used to measure the magnetic flux density by inserting a probe between the wheel rim and the steel pipe. A seat for the probe with a volume of $3.15 \times 0.5 \times 8.0$ mm^3 is made by milling away on a pipe surface. It is impossible measure flux density with a gap of 0 mm since there exists no gap between the wheel and the steel pipe in practice. This is the reason to use the compensation equations, which are derived by using the simulation and experimental data.

The detailed experimental procedure for the latter experiments is as follows. A steel pipe with a diameter of 100 mm

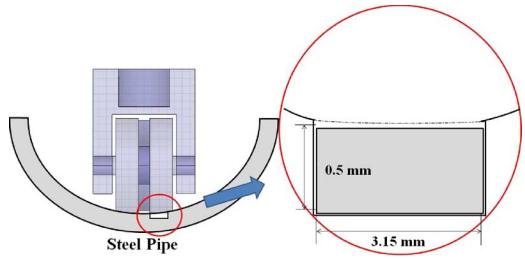

Fig. 5. Experimental setup for the measurement of flux density.

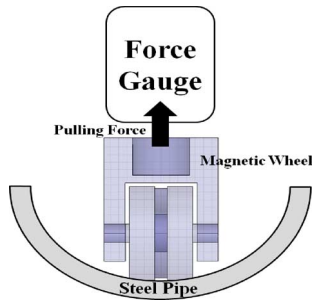

Fig. 6. Experimental setup for the measurement of magnetic force.

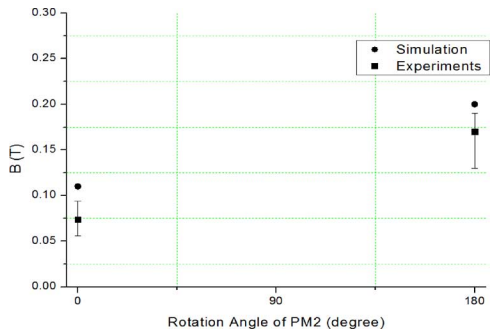

Fig. 7. Flux density change to the change of rotated angle of PM2 when applied a gap.

is cut in half and securely fastened on the table. The magnetic wheel is placed on the center of the half pipe, and then the digital push-pull gauge (DS2-50N) is hooked onto the magnetic wheel. The measurements are conducted at an interval of 30°. To rotate PM2 at a specific angle, corresponding PWM signals are sent to the servo motor. At every angle, the measurements are repeated three times, which are averaged and plotted.

Fig. 7 shows the plot of the simulated and experimental flux density with respect to the rotation of PM2. The experimental and simulated flux density increases according to the rotation of the PM2. The maximum flux density is 0.21 T, and the minimum flux density is 0.11 T, in simulation. In the experiments, using a gauss meter to measure magnetic flux density, the maximum flux density is 0.17 T, and the minimum flux density is 0.07 T.

Table I is the summary of flux density variation according to the change of a gap in simulation, experiments and compensation.

Fig. 8 shows the simulated, mathematics and experimental magnetic forces with respect to the rotation of PM2. The experimental magnetic force increases almost linearly according to the rotation of PM2, while the simulated magnetic force remains

TABLE I
FLUX DENSITY VARIATION ACCORDING TO THE CHANGE OF GAP

Degree	Simulation		Experiments		Compensation	
	0 mm	0.5 mm	0 mm	0.5 mm	0 mm	0.5 mm
0°	0.71 T	0.11 T	N/A	0.07 T	0.67 T	0.07 T
180°	1.19 T	0.21 T	N/A	0.17 T	1.15 T	0.17 T

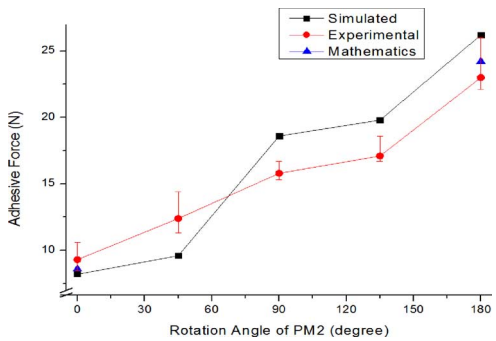

Fig. 8. Magnetic force change to the change of rotated angle of PM2.

TABLE II
MAGNETIC FORCE COMPARISON BETWEEN THE METHODS USED

Degree	Magnetic Force (Mathematics)	Magnetic Force (Simulation)	Magnetic Force (Experiments)
0°	8.6 N	8.2 N	9.3N
15°		8.5 N	
30°		9.3 N	
45°		9.6 N	12.4 N
60°		12.2 N	
75°		12.4 N	
90°		18.6 N	15.8 N
105°		19.1 N	
120°		19.6 N	
135°		19.8 N	17.1 N
150°		22.4 N	
165°		23.7 N	
180°	24.2 N	26.2 N	23 N

almost constant up to 45°, then increases with further rotation of PM2.

The magnetic forces with the adhered-state and with the free-state are estimated as 8.20 and 26.20 N, respectively in simulation. In the experiment, the magnetic forces with the adhered-state and with the free-state are estimated as 9.30 and 23 N. Mathematically, the magnetic forces with the adhered-state and with the free-state are estimated as 8.6 and 24.2 N, respectively.

Table II is the summary of the magnetic force comparison between the methods used. The difference between the calculated and measured magnetic force may be explained by the fact that the mathematical model does not include flux leakage.

MAXWELL-3D can represent the actual model most clearly, but MAXWELL-3D simulation results are similar but not the same as the experimental results.

IV. CONCLUSION

This paper proposes a new controllable magnetic wheel. The idea is conceptualized, simulated, fabricated, and validated experimentally.

The MAXWELL-3D results confirm that the iron wheel rims and PM2 acts as an extension and keeper of the PM1, or vice versa. The magnetic wheel is made and subjected to the experiments. From the experiments, it is clear that the magnetic force increases as the PM2 rotation increases.

In the experiments, a gauss meter is used to measure the flux density between the magnetic wheel rim and steel pipe. The compensation equation is derived and applied to correct the simulation and experimental data. As a result, in simulation, the flux density changed from 0.11 to 0.21 T with a gap of 0.5 mm. Also, in the experiments, the flux density changed from 0.07 to 0.17 T with a gap of 0.5 mm. As a compensation result, in the experiments, the flux density changed from 0.67 to 1.15 T, which means that the proposed method is effective to control magnetic force between the wheel and interior surfaces of the ferromagnetic pipes. The developed magnetic wheels may be smaller and reliable than those in the literature [2]–[5] from a design point of view. Continuous control of the magnetic force may be beneficial to lighten the burden on the driving motor.

ACKNOWLEDGMENT

This work was supported in part by the Korea Institute of Energy Research under Grant 20101020100130.

REFERENCES

[1] B. S. Chu, K. M. Jung, C. S. Han, and D. H. Hong, "A survey of climbing robots: Locomotion and adhesion," *Int. J. Precision Eng. Manuf.*, vol. 11, no. 4, pp. 633–647, 2010.

[2] W. Fischer, F. Tache, and R. Siegwart, "Magnetic wall climbing robot for thin surfaces with specific obstacles," in *Proc. Int. Conf. Field Service Robot.*, Chamocix, France, Jul. 2007.

[3] W. Fischer, G. Caprari, R. Siegwart, and R. Moser, "Compact magnetic wheeled robot for inspecting complex shaped structures in generator housings and similar environments," presented at the IEEE/RSJ Int. Conf. Intell. Robots Syst., St. Louis, MO, Oct. 2009.

[4] Y. Kawaguchi, I. Yoshida, H. Kurumantani, T. Kikuta, and Y. Yamada, "Internal pipe inspection robot," presented at the IEEE Int. Conf. Robot. Automat., Nagoya, Japan, May 1995.

[5] S. C. Han, J. H. Kim, and H. C. Yi, "A novel design of permanent magnet wheel with induction pin for mobile robot," *Int. J. Precision Eng. Manuf.*, vol. 10, no. 4, pp. 143–146, 2009.